Scaling of G1 Duration with Population Doubling Time by a Cyclin in *Saccharomyces cerevisiae*

Heidi M. Blank,[1] Michelle Callahan, Ioannis P. E. Pistikopoulos, Aggeliki O. Polymenis,[2] and Michael Polymenis[1]

Department of Biochemistry and Biophysics, Texas A&M University, College Station, Texas 77843

ORCID IDs: 0000-0002-2251-5246 (H.M.B.); 0000-0003-1507-0936 (M.P.)

ABSTRACT The longer cells stay in particular phases of the cell cycle, the longer it will take these cell populations to increase. However, the above qualitative description has very little predictive value, unless it can be codified mathematically. A quantitative relation that defines the population doubling time (T_d) as a function of the time eukaryotic cells spend in specific cell cycle phases would be instrumental for estimating rates of cell proliferation and for evaluating introduced perturbations. Here, we show that in human cells, the length of the G1 phase (T_{G1}) regressed on T_d with a slope of ≈0.75, while in the yeast *Saccharomyces cerevisiae*, the slope was slightly smaller, at ≈0.60. On the other hand, cell size was not strongly associated with T_d or T_{G1} in cell cultures that were proliferating at different rates. Furthermore, we show that levels of the yeast G1 cyclin Cln3p were positively associated with rates of cell proliferation over a broad range, at least in part through translational control mediated by a short upstream ORF (uORF) in the *CLN3* transcript. Cln3p was also necessary for the proper scaling between T_{G1} and T_d. In contrast, yeast lacking the Whi5p transcriptional repressor maintained the scaling between T_{G1} and T_d. These data reveal fundamental scaling relationships between the duration of eukaryotic cell cycle phases and rates of cell proliferation, point to the necessary role of Cln3p in these relationships in yeast, and provide a mechanistic basis linking Cln3p levels to proliferation rates and the scaling of G1 with doubling time.

KEYWORDS cell size; growth law; START; chemostat

RECURRING shapes and patterns in nature are sometimes described by mathematical relationships. As a result, these natural processes can be predicted and understood better. Regarding patterns of eukaryotic cell division, one could ask: how are the lengths of eukaryotic cell cycle phases related to each other and to the total doubling time of the population? Can such relationships be described mathematically, in the form of a scaling formula? If so, what are the molecular mechanisms that govern the scaling? A scaling relationship that describes eukaryotic cell division would be a significant advance. For example, it could serve as a point of reference against which the effects of genetic or other perturbations can be evaluated.

The "textbook" view in the coordination of growth and division in the eukaryotic cell cycle [*e.g.*, see figures 10–26 in Morgan (2007)] is that expansion of the G1 phase of the eukaryotic cell cycle accounts for most, if not all, of the lengthening of the cell cycle in slower-proliferating cells in budding yeast (Johnston *et al.* 1977; Brauer *et al.* 2008) or humans (Baserga 1985; Fisher 2016). However, there is no report in the literature of a quantitative relationship that defines the doubling time (T_d) as a function of the time that yeast or human cells spend in the G1 phase (T_{G1}). Here, based on all the available data for budding yeast and human cell populations, we derived for the first time in the field scaling relationships between T_{G1} and T_d. These scaling relationships also allowed us to critically evaluate the role of cell cycle regulators in yeast cells proliferating at different rates.

Two key regulators of the length of the G1 phase in *Saccharomyces cerevisiae* are the Cln3p and Whi5p proteins. The G1 cyclin Cln3p promotes the initiation of DNA replication (Cross 1988; Nash *et al.* 1988). In contrast, the transcriptional

doi: https://doi.org/10.1534/genetics.118.301507
Manuscript received June 29, 2018; accepted for publication August 24, 2018; published Early Online August 27, 2018.
Supplemental material available at Figshare: https://figshare.com/articles/Supplemental_Data/7011275.
[1]Corresponding authors: Department of Biochemistry and Biophysics, Texas A&M University, 300 Olsen Blvd., 2128 TAMU, College Station, TX 77843-2128. E-mail: HeidiBlank@tamu.edu; and polymenis@tamu.edu
[2]Present address: Department of Physics and Astronomy, University of California, Los Angeles, CA 90095.

repressor Whi5p acts analogously to the retinoblastoma gene product in animals to inhibit the G1/S transition (Costanzo *et al.* 2004; de Bruin *et al.* 2004; Palumbo *et al.* 2016). It has been reported that while synthesis of Cln3p parallels cell size, the synthesis of Whi5p is independent of cell size (Schmoller *et al.* 2015), arguing that dilution of Whi5p as cells get bigger in G1 governs the length of the G1 phase (Schmoller and Skotheim 2015; Schmoller *et al.* 2015).

Here, we obtained the first measurements of Cln3p and Whi5p levels as a function of proliferation rates in steady-state cultures. The levels of Cln3p varied over a broad range, due to an upstream ORF (uORF) affecting translation of *CLN3*. Our data also show that loss of Whi5p does not significantly affect the scaling relationship between T_d and T_{G1}. Instead, we provide strong evidence for the functional and molecular basis of the necessary role of Cln3p in this process.

Materials and Methods

Strains

Unless stated otherwise, *S. cerevisiae* wild-type, *cln3*Δ, and *whi5*Δ *strains* were in the BY4741 background [National Center for Biotechnology Information (NCBI) Taxonomy 559292; *MAT***a**, *his3*Δ*1*, *leu2*Δ*0*, *ura3*Δ*0*, *met15*Δ*0*), and they have been described previously (Soma *et al.* 2014). For protein surveillance, we constructed an otherwise wild-type strain that carried epitope-tagged *WHI5* and *CLN3* alleles at their endogenous chromosome locations. First, a commercially available *WHI5-TAP*::*HIS3* strain (BY4741 otherwise; GE Healthcare) was backcrossed three times into the W303 background (NCBI Taxonomy 580240; *MAT*α *leu2-3,112 trp1-1 can1-100 ura3-1 ade2-1 his3-11,15*). Then, it was crossed with an otherwise wild-type strain carrying a *CLN3-13MYC* allele (W303 background), described elsewhere (Thorburn *et al.* 2013), and kindly provided by A. Amon (Massachusetts Institute of Technology and Howard Hughes Medical Institute). The resulting diploid was sporulated and dissected to obtain *MAT***a** haploid segregants carrying both the epitope-tagged *WHI5* and *CLN3* alleles (strains HB94/97; *MAT***a** *CLN3-13MYC*::*TRP*$^+$ *WHI5-TAP*::*HIS*$^+$ *leu2 ura3 met15*), which were used in the experiments shown in Figure 4. We verified expression of Whi5p-TAP and Cln3p-$(Myc)_{13}$ in this strain (see Supplemental Material, File S1), and their absence in *whi5*Δ or *cln3*Δ strains, respectively. We also generated a derivative of this strain, which lacks the uORF in the 5′-leader of the *CLN3* mRNA. To this end, we used plasmid A-315T-pMT10, which we have described previously (Polymenis and Schmidt 1997), as a template in a PCR reaction with forward (5′-CAAGAACTACCATTCGACAGG-3′) and reverse primers (5′-CGTACAGAAAGCGTATCAAA-3′) to generate a product that carries the *URA3*-marked A-315T mutation, which inactivates the uORF, in the 5′-leader of *CLN3*. We then used this PCR product to transform strain HB94 (*WHI5-TAP* and *CLN3-13MYC*). Genomic DNA of transformants was sequenced to verify the presence of the A-315T mutation. Confirmed A-315T mutants were then backcrossed with wild-type cells (W303) to segregate away possible secondary mutations at other loci. The resulting heterozygote was sporulated and dissected to isolate a *WHI5-TAP*, *A-315T-CLN3-13MYC* segregant (HB104), which was used in the experiments shown in Figure 4.

Data sets for population-based cell cycle parameters

All the obtained variables that we report here represent population averages. They do not resolve intergenerational differences in cell cycle progression of the same cells in successive cell cycles. In the context of this study, population averages hold significant advantages: first, they are easily obtained; second, they are ubiquitously used and reported in the literature; and third, they allow straightforward comparisons between different systems, for example between yeast and human cells (see Figure 1).

For yeast, the data we collected (Table S1) were from wild-type strains from various backgrounds, except in the few cases where they carried temperature-sensitive alleles, such as *cdc* mutations (Jagadish and Carter 1977), to estimate the length of the G1 phase upon transfer to the nonpermissive temperature. The methods used to calculate the fraction of G1 cells included: measurements of the DNA content of the cells by flow cytometry (Slater *et al.* 1977; Johnston *et al.* 1980; Guo *et al.* 2004; Brauer *et al.* 2008; Henry *et al.* 2010); budding (Tyson *et al.* 1979; Rivin and Fangman 1980), sensitivity to cell cycle arrest before DNA replication by pheromone (Hartwell and Unger 1977; Jagadish and Carter 1977), or *cdc* (Jagadish and Carter 1977) mutations. In this study, to obtain the fraction of G1 cells (*e.g.*, see Figure 3 and Figure 4), we used DNA content measurements by flow cytometry, as described previously (Hoose *et al.* 2012, 2013).

For human cells, earlier studies employed ^{3}H-thymidine pulses or division waves after thymidine block (Baserga 1985). The doubling times of the NCI-60 human cancer cell lines that we included in Table S2 are known (Ross *et al.* 2000; Scherf *et al.* 2000; Polymenis 2017), but there was no quantitative cell cycle data for most of the cell lines. However, images of DNA content profiles for the NCI-60 panel, albeit with no quantification, have been published (Garner and Eastman 2011). We requested and obtained high-resolution files of these images from Alan Eastman (Geisel School of Medicine, Dartmouth College). From the entire DNA content histogram, to quantify the fraction of cells in G1, we used imaging software to measure the area on the left side of the G1 peak (from peak to valley) and multiplied this area by two, as has been described previously (Johnston *et al.* 1980). This approach avoids complications from heavy right-side tails due to S phase cells and yields an acceptable estimate of the relative G1 length as a fraction of total cell cycle time. We then combined these values with all others available from human cells, cancerous and normal (Sisken and Kinosita 1961; Defendi and Manson 1963; Lennartz and Maurer 1964; Aoki and Moore 1970; Baserga 1985; Kumei *et al.* 1989; Brons *et al.* 1992; Luciani *et al.* 2001; Hahn *et al.* 2009), to compile a data set of 96 values for G1 length (T_{G1}) and doubling time (T_d) for human cells, shown in Table S2.

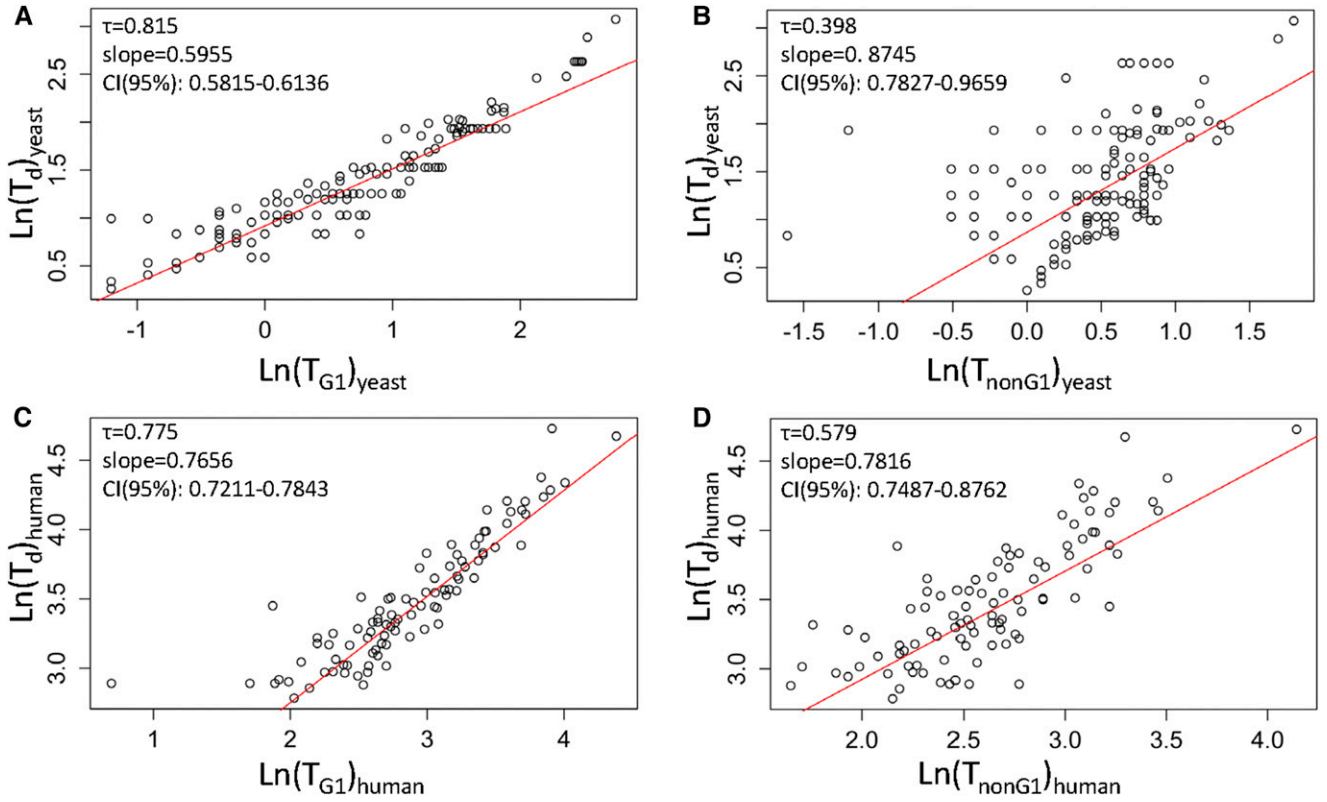

Figure 1 Linking the length of the G1 phase with population doubling time. Scatter plots of T_{G1} (A and C) or T_{nonG1} (B and D) values on the *x*-axis, against T_d values (*y*-axis). All plots used the natural logarithms (Ln) of the values for yeast (A and B) and human (C and D) cells from Tables S1 and S2, respectively. The Kendall's (τ) rank correlation coefficient is shown in each case. In red are regression lines of the Siegel repeated medians. The slope and the associated 95% C.I.s of the linear model are shown in each case. Additional statistical parameters associated with these plots are shown in Table 1.

Estimates of G1 length

The values we show in Tables S1 and S2 were obtained from studies reporting on the relative duration of the G1 phase. To estimate the *absolute* length of the G1 phase, T_{G1}, we multiplied the relative G1 length by T_d (Tables S1 and S2). This simple equation is the appropriate one to use with chemostat data when as many cells are removed as are being produced in the culture (Hoffman 1949). Subtracting T_{G1} from T_d yields the duration of the rest of the cell cycle phases (T_{nonG1}). For nonchemostat data, other more elaborate equations could be used, especially for the asymmetric patterns of division of budding yeast (Hartwell and Unger 1977; Johnston *et al.* 1980). However, for simplicity and ease of comparison across systems, we uniformly applied the simple equation mentioned above. Furthermore, inaccuracies in the absolute values of T_{G1} may only affect the intercept of the linear relationship between T_d and T_{G1}, but not the slope that describes the fundamental scaling between T_d and T_{G1}, or any of our conclusions. Indeed, when we plotted in the same manner as in Figure 1 only the chemostat values in Table S1 (94 data points), the slope of $LnT_d \propto LnT_{G1}$ was 0.6107. For the remaining, nonchemostat values (55 data points), the slope of $LnT_d \propto LnT_{G1}$ was 0.6074.

Lastly, a limitation of the nonchemostat data in yeast and all the data from human cells is that it is assumed that cell death contributes negligibly to the doubling time of the population. This assumption is reasonable in yeast because young cells vastly outnumber older ones approaching senescence. However, it may be of concern in mammalian culture systems. Hence, our data with human cells should be interpreted with caution, because the fraction of growing cells in the culture may be significantly lower than one. Also, although we are looking at trends that seemingly hold across a multitude of human cell types, the data were overwhelmingly derived from cancer cell lines, which in many cases have altered cell cycles.

Chemostat cultures

The experiments were done using a New Brunswick BioFlo (BF-110) reactor with a working volume of 880 ml. The reactor was run at room temperature, as described earlier (Henry *et al.* 2010). In each experiment and at each dilution rate, the reactor was sampled several times to measure protein levels by immunoblots, the DNA content with flow cytometry, and the cell size and cell density of the culture using a Beckman Z2 channelyzer (Henry *et al.* 2010; Hoose *et al.* 2012), as indicated. We measured the cell density at every sampling to ensure that we never reached "wash-out" conditions at the high dilution rates. In every experiment, the cell density remained $>$ 1E+07 cells/ml, and did not vary more than threefold between the lowest and highest dilution rates.

Protein surveillance

Proteins were resolved onto 4–12% Tris-glycine gels (catalog number: XP04125BOX; Thermo Scientific). Cln3p-$(Myc)_{13}$ was detected with an anti-Myc antibody (catalog number: ab13836; Abcam). All other procedures for TAP-tagged protein detection, extract preparation for immunoblots, and their analysis have been described elsewhere (Blank *et al.* 2017).

Statistical analysis

Data were analyzed and displayed with R language packages. All R functions, the corresponding packages, and their use are listed in Table S3. To build the linear models we described using the values for the yeast (Table S1) and human (Table S2) data sets, we first examined if the assumptions for building simple, linear parametric models were satisfied. The diagnostic residual plots evaluating whether the errors were independent of each other, normally distributed around a mean of zero and equal variance, are shown in Figure S2. In both the yeast and human data sets, the existence of a few outlier points appeared to violate the necessary assumptions [Figure S2; $P < 0.05$ for assessment of the assumptions using the global test on four d.f. (Peña and Slate 2006)]. Hence, we opted for nonparametric, robust linear regression models based on Siegel repeated medians (Table 1). For the meta-analysis of cell size data (see Figure 2) we used the *metafor* R language package (Viechtbauer 2010). Briefly, the correlation coefficients from each study were transformed using Fisher's z transformation. An unbiased random effects analysis, as opposed to a fixed effects one, was then performed using this index, and the summary values were converted back to correlations and displayed as such with "forest" plots (Figure 2 and Table S3).

Data availability

Strains and plasmids are available upon request. The authors affirm that all data necessary for confirming the conclusions of the article are present within the article, figures, and tables. Figure S1 shows goodness-of-fit plots for lognormal distribution of yeast and human T_{G1} values. Figure S2 shows diagnostic plots of simple linear regression models for T_d and T_{G1} values of yeast and human cells. Figure S3 shows additional chemostat experiments with *whi5Δ* and *cln3Δ* cells. Table S1 lists all the cell cycle values for yeast cells from the literature. Table S2 lists all the cell cycle values for human cells from the literature. Table S3 lists all R functions, the corresponding packages, and their use. File S1 contains all raw immunoblot images generated and used in this study. Supplemental material available at Figshare: https://figshare.com/articles/Supplemental_Data/7011275.

Results

Rationale

The rationale for the experiments we describe was the following. First, use all the available values from the literature to derive a quantitative relationship of the population doubling time (T_d) as a function of the time eukaryotic cells spend in the G1 phase of the cell cycle (T_{G1}) (Figure 1). Second, based on the same data sets and analyses, examine if cell size is also related to T_d or T_{G1}, because cell size is often used as a proxy for the control of cell division by nutrients (Figure 2). Third, use the linear relationship linking T_d and T_{G1} as a metric to evaluate the contributions of Whi5p and Cln3p, two proteins that govern the G1/S transition in budding yeast (Figure 3). Fourth, if Cln3p or Whi5p impinges on the relationship between T_d and T_{G1}, then provide a mechanistic understanding of its role (Figure 4).

T_{G1} values are distributed lognormally, consistent with exponential patterns of growth

We compiled the available values for T_d and T_{G1} from the literature for budding yeast (Table S1) and human (Table S2) cells (see *Materials and Methods*). With the data set of T_{G1} values at hand, we next examined their distribution. Knowing how the T_{G1} values are distributed will inform how to better model T_{G1} against T_d and offer some insight into the processes that determine G1 length. We found that T_{G1} values were not normally distributed for yeast ($P = 4.434E{-}14$, Shapiro–Wilk test) or human cells ($P = 1.039E{-}07$, Shapiro–Wilk test). Instead, T_{G1} values fit a lognormal distribution better. For example, for yeast T_{G1} values, the Anderson–Darling statistic was the lowest for the lognormal distribution (0.347) compared to other distributions (Weibull: 1.693; γ: 1.521; exponential: 2.462). As expected for lognormal distributions, log-transformed values of T_{G1} were normally distributed for yeast (Figure S1, A–D, $P = 0.1871$, Shapiro–Wilk test) and human cells (Figure S1, E–H, $P = 0.3099$, Shapiro–Wilk test). The apparent lognormal distribution of T_{G1} values is consistent with a multiplicative process of many, positive, independent random variables that determine the G1 length (Koch 1966). Lognormal distributions are very common in biological growth processes (Mosimann and Campbell 1988). In cell proliferation, lognormality has been proposed to reflect exponential patterns of growth in mass. Despite fluctuations in the growth rate constant, the growth of the overwhelming majority of cellular components is influenced similarly, leading to lognormality (Koch and Schaechter 1962; Koch 1966). In budding yeast and other cell types, there is evidence for exponential patterns of protein synthesis (Elliott and McLaughlin 1978; Di Talia *et al.* 2007; Tzur *et al.* 2009) and increase in mass in the cell cycle (Bryan *et al.* 2012; Son *et al.* 2012). Such considerations accommodate the lognormality of T_{G1} values we describe here.

Strong association between T_{G1} and T_d, but non-G1 phases also expand in lower proliferation rates

To test for association between T_{G1} and T_d, we used the distribution-free Spearman's and Kendall's tests for independence based on ranks. We used these nonparametric, distribution-free tests because of the existence of outliers even in

Table 1 Statistical parameters of linear relationships

Variables		Coefficients[a]		Confidence intervals (level = 0.95)					
				Intercept		Slope			
Y	X	Intercept	Slope					τ^b	r^c
$(T_d)_{yeast}$	$(T_{G1})_{yeast}$	1.429	1.091	1.3817	1.5049	1.0598	1.1133	0.815	0.938
$(T_d)_{yeast}$	$(T_{nonG1})_{yeast}$	0.36	1.75	0.1900	0.8712	1.6244	2.0278	0.398	0.532
$Ln(T_d)_{yeast}$	$Ln(T_{G1})_{yeast}$	0.9168	0.5955	0.9047	0.9418	0.5815	0.6136	0.815	0.938
$Ln(T_d)_{yeast}$	$Ln(T_{nonG1})_{yeast}$	0.8682	0.8745	0.7764	0.9128	0.7827	0.9659	0.398	0.532
$(T_d)_{human}$	$(T_{G1})_{human}$	7.558	1.279	6.8401	8.5971	1.2433	1.3339	0.775	0.921
$(T_d)_{human}$	$(T_{nonG1})_{human}$	6.838	1.738	3.6212	7.3905	1.6919	2.0059	0.579	0.762
$Ln(T_d)_{human}$	$Ln(T_{G1})_{human}$	1.2202	0.7656	1.1770	1.3663	0.7211	0.7843	0.775	0.921
$Ln(T_d)_{human}$	$Ln(T_{nonG1})_{human}$	1.3608	0.7816	1.1374	1.4674	0.7487	0.8762	0.579	0.762
$Ln(T_d)_{whi5\Delta}$[d]	$Ln(T_{G1})_{whi5\Delta}$[d]	1.1654	0.6166	1.1613	1.1910	0.6083	0.6362	0.928	0.987
$Ln(T_d)_{HB94/7}$[e]	$Ln(T_{G1})_{HB94/7}$	0.9691	0.6848	0.9031	0.9843	0.6588	0.7461	0.765	0.918
$Ln(T_d)_{HB104}$[f]	$Ln(T_{G1})_{HB104}$	0.9913	0.7048	0.9902	1.0074	0.6930	0.7120	0.934	0.989

T_d, population doubling time; T_{G1}, length of the G1 phase; T_{nonG1}, length of the cell cycle excluding G1 phase; LN, natural logarithm.
[a] From the linear fit of Siegel repeated medians.
[b] Kendall's (τ) rank correlation coefficient.
[c] Spearman's (r) rank correlation coefficient.
[d] The values for *whi5*Δ cells were from the experiment shown in Figure 3B.
[e] The values for HB94/7 cells (*CLN3-13MYC*, *WHI5-TAP*) were from the experiments in Figure 4A.
[f] The values for HB104 cells (*A-315T-CLN3-13MYC*, *WHI5-TAP*) were from the experiments in Figure 4B.

log-transformed T_{G1} values (*e.g.*, see Figure S1). The high values (> 0.75) of the rank correlation coefficients (τ for Kendall's and r for Spearman's; see Table 1) show a strong positive association between T_{G1} and T_d, for both yeast (Figure 1A) and human (Figure 1C) cells. However, interestingly, the duration of the non-G1 phases (T_{nonG1}) of the cell cycle were also positively correlated with T_d (Figure 1, B and D and Table 1) in both organisms, albeit less so in yeast ($\tau = 0.398$; Figure 1B) than in human cells ($\tau = 0.579$; Figure 1D). Overall, our data document the strong association between T_{G1} and T_d (Figure 1, A and C). Additionally, they suggest that growth requirements for cell division are not registered exclusively in G1, but also later in the cell cycle (see Figure 1, B and D), in agreement with observations from other groups (Anastasia *et al.* 2012; Ferrezuelo *et al.* 2012; Dowling *et al.* 2014; Soifer and Barkai 2014; Cerulus *et al.* 2016; Mayhew *et al.* 2017; Garmendia-Torres *et al.* 2018).

A scaling relationship between T_{G1} and T_d

To estimate a predictive and quantitative relationship between T_{G1} and T_d, we derived nonparametric, robust linear regression models using the Siegel repeated median estimates (Siegel 1982) (Figure 1 and Table 1; see also *Materials and Methods*). The intercepts of the linear T_{G1} *vs.* T_d plots reflect the apparent minimum duration of the S+G2+M phases in yeast (1.4 hr; Table 1) and human (7.6 hr; Table 1) cells. The slopes in the linear relationships indicate how much T_d is affected by T_{G1} or T_{nonG1}. For example, if non-G1 phases were not expanding in slower-proliferating cells, then one would expect a vertical line parallel to the *y*-axis in T_{nonG1} *vs.* T_d plots. We noticed that the slope of the regression of T_{G1} on T_d appeared to slightly differ between the yeast and human data sets (Figure 1 and Table 1). Applying the nonparametric Sen–Adichie test for parallelism confirmed that the difference in the slopes of the regression lines of T_{G1} on T_d between yeast and human cells was statistically significant (V statistic = 7.324, *P*-value = 0.007). Although the T_{G1} distributions themselves are lognormal, log-transformation is not necessary for any of our conclusions, since we used a nonparametric, ordinal-based analysis in all our statistical tests. Nonetheless, we display regression plots using log-transformed data to improve visualization, because data points appear more evenly on these graphs. Furthermore, log-transformed values are often incorporated in scaling relationships between the measured variables in the literature (Chan and Marshall 2010). The quantitative relationships that we identified linking T_{G1} with T_d are significant because they provide a framework to interpret experimental perturbations in cell cycle progression and cell proliferation, as we will describe for yeast cells.

Nutrient-specific, but not growth rate-dependent, association between cell size and T_{G1}, or T_d

Control of cell size has frequently been used synonymously with growth control of G1 transit in the cell cycle, especially in budding yeast. Daughter cells of *S. cerevisiae* are born smaller than their mother is, and they will not initiate a new round of cell division until they reach a size characteristic of the culture medium. The rate at which daughter cells increase in volume has been reported to contribute to the size at which they will initiate a new round of cell division (Ferrezuelo *et al.* 2012). Note that unless indicated otherwise, here we use the term growth rate to describe the rate at which cells proliferate and not the rate at which they increase in size in a given cell cycle. As the cell cycle is prolonged in poor nutrients, it is also widely assumed that the cells get smaller [*e.g.*, see figures 10–26 in Morgan (2007)]. To test the strength of the association between cell size and T_{G1}, or T_d, we combined the available data from previous studies (Tyson *et al.* 1979; Guo *et al.* 2004; Brauer *et al.* 2008; see Table S1). From such an unbiased but unweighted analysis (Figure 2, A and D), it appeared that the size of yeast cells was not significantly associated with T_d (*P*-value = 0.171, based on Kendall's test; Figure 2A) or T_{G1} (*P*-value = 0.2449, based on Kendall's test; Figure 2D).

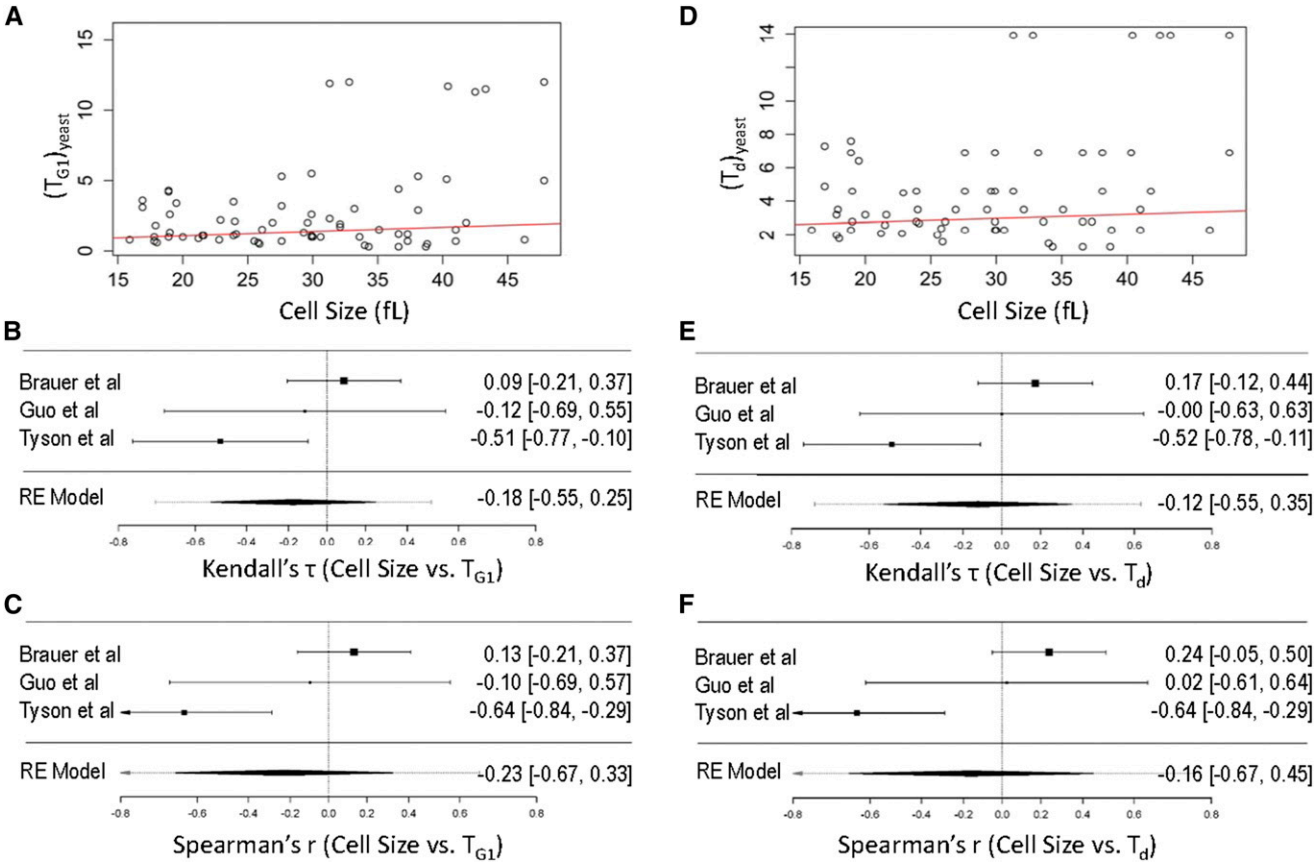

Figure 2 Cell size does not correlate with T_d or T_{G1} in yeast. Scatter plots of cell size values (*x*-axis) against T_d (A) or T_{G1} (D) values (*y*-axis) from the data shown in Table S1. In red are regression lines of the Siegel repeated medians. Forest plots of the measure of effect for each of the studies included in the analysis (Tyson *et al.* 1979; Guo *et al.* 2004; Brauer *et al.* 2008), based on the Kendall's (τ) rank correlation coefficients (B and E) or Spearman's (r) rank correlation coefficients (C and F), are shown in each case, for cell size *vs.* T_{G1} (B and C) and cell size *vs.* T_d (E and F). The C.I.s from each study are shown in parentheses and represented by horizontal whisker lines. In the studies in which the confidence intervals overlap with the vertical line at the 0 point on the *x*-axis, their effect sizes do not differ from no effect. The meta-analyzed measure of the effect is shown at the bottom of each plot, based on random effects (RE) models.

Unlike the strong association of T_{G1} with T_d, which was consistent across studies (see Figure 1 and *Materials and Methods*), the association between cell size and T_{G1}, or T_d, appeared to vary among the relevant studies. Given the different number of samples analyzed in each study and their associated variance, we calculated the effect sizes from each study separately, based on the nonparametric Spearman's and Kendall's correlation coefficients. These study-specific correlation coefficients then served as the effect size index, to standardize the different studies and arrive at a summary correlation (Borenstein 2009). The results were visualized in typical forest plots (Figure 2, B, C, E, and F). A negative association between size and rates of cell proliferation, with cells getting smaller with larger T_d values, was only evident at a moderate level in batch cultures ($\tau = -0.52$, $r = -0.64$; see Figure 2, E and F), where different nutrients were used to achieve different doubling times (Tyson *et al.* 1979). In contrast, in other studies (Guo *et al.* 2004; Brauer *et al.* 2008), which employed chemostats to alter the population doubling time independently of the limiting nutrient, there was no correlation between cell size and T_d, or T_{G1} (Figure 2). Importantly, within these chemostat studies, cell size measurements were internally calibrated. Hence, the lack of any correlation between cell size and T_d, or T_{G1} cannot be attributed to experimental variabilities of different studies incorporated in our meta-analysis of the literature. Lastly, the lack of a significant association between T_{G1} and cell size agrees with a genome-wide survey of single-gene deletions (Hoose *et al.* 2012), which found no pattern of correlation between cell size and the relative duration of the G1 phase. Hence, although cell size can be modulated by changes in nutrient composition in yeast (Tyson *et al.* 1979; Soma *et al.* 2014; and others), our data suggest that it is more likely that these are nutrient-specific effects, not causally linked to changes in cell proliferation rates.

Cln3p, but not Whi5p, is required for the strong association between T_{G1} and T_d

To understand how the relationship between the length of the G1 phase and doubling time is established in budding yeast,

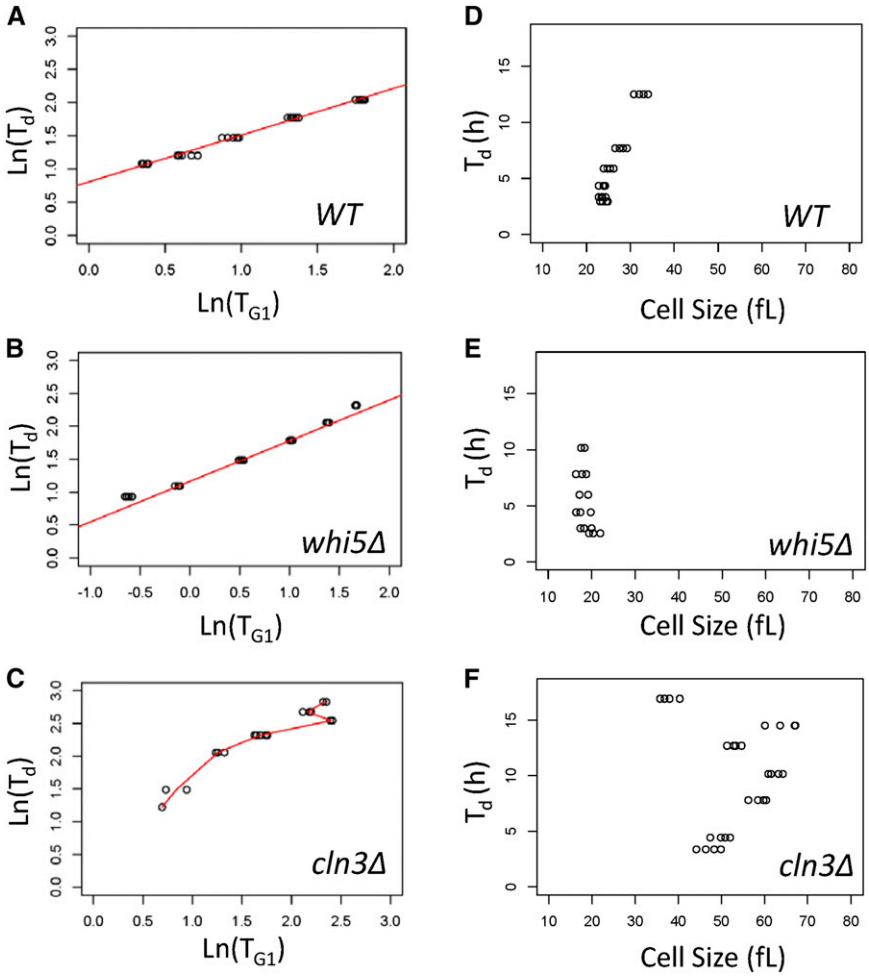

Figure 3 Cln3p, but not Whi5p, imposes the proper relationship between T_{G1} and T_d. Scatter plots of T_{G1} values on the *x*-axis against T_d values (*y*-axis). All plots used the natural logarithms (Ln) of the values for wild-type (WT) (A), *whi5Δ* (B), or *cln3Δ* (C) cells, sampled from chemostat cultures several times at each dilution rate, as indicated. For WT and *whi5Δ* cells, regression lines of the Siegel repeated medians are in red and the slope of the linear models are shown (additional statistical parameters are in Table 1). For *cln3Δ* cells, the red line shown simply connects the average values at each dilution rate. There is no regression line because the relationship between T_d and T_{G1} breaks down, especially at longer generation times. Scatter plots of the relationship of cell size and T_d in WT (D) or cells lacking Whip5 (E) or Cln3p (F), with cell size values (*x*-axis) plotted against T_d (*y*-axis) from the same cultures described in (A–C). All the strains were in the BY4741 background (see *Materials and Methods*).

we next examined the role of the Cln3p and Whi5p proteins, which regulate the G1/S transition in this organism. It has been proposed that dilution of Whi5p as cells get bigger in G1 is the key event controlling the timing of the G1/S transition (Schmoller and Skotheim 2015; Schmoller *et al.* 2015). Since in cells proliferating at different rates there is not a significant correlation with cell size (Figure 2 and Table S1), it is not clear how the inhibitor dilution model would apply to the conditions we examined in this study. To our knowledge, the kinetics of cell cycle progression in cells lacking Cln3p or Whi5p have not been examined previously in steady-state cultures proliferating at different rates. To test the role of Cln3p and Whi5p in the relationship between T_{G1} and T_d, we examined the cell cycle profile of *cln3*Δ or *whi5Δ* cells in continuous, steady-state chemostat cultures. We measured T_{G1} in *cln3Δ* or *whi5Δ* cells from the DNA content of the cultures under glucose (0.08% $^{w}/_{v}$) limitation and at different dilution rates (0.038–0.348 hr^{-1}; corresponding to T_d values between 18 and 2 hr, respectively). As expected, cells lacking Whi5p were very small (≈18 fl) and their size did not change significantly as a function of T_d (Figure 3E and Figure S3D). Furthermore, the intercept of the linear fit between the log-transformed T_d and T_{G1} values of *whi5*Δ cells was significantly higher than the intercept of the linear fit of these parameters in wild-type cells (1.17 *vs.* 0.92; see Table 1), consistent with the shortened G1 phase of *whi5*Δ cells. The slope of the linear relationship between T_d and T_{G1} in *whi5Δ* cells (Figure 3B) was similar to what we observed in the aggregate analysis of wild-type cells (Figure 1A and Table 1; Sen–Adichie V statistic = 1.775, *P*-value = 0.183), albeit slightly smaller than the slope of wild-type cells from a separate, independent experiment performed in this study [0.6723 in wild-type (Figure 3A) *vs.* 0.6166 in *whi5Δ* cells (Figure 3B)]. These data suggest that in different physiological states, and despite their shortened G1 phase and small size, *whi5Δ* cells nonetheless remain responsive to different environments, displaying minimal changes in their scaling of the expected proportional changes between T_d and T_{G1}.

In contrast, cells lacking Cln3p had an abnormal behavior. In three independent experiments (Figure 3C and Figure S3, B and C), T_{G1} did not even have a straightforward linear relationship with T_d in cultures of *cln3*Δ cells. At shorter division times (T_d < 5 hr), the T_d and T_{G1} values of *cln3*Δ cultures were related linearly, albeit with a higher slope (*e.g.*, Figure S3C; slope = 0.7685). More importantly, in all three independent experiments, the linear relationship

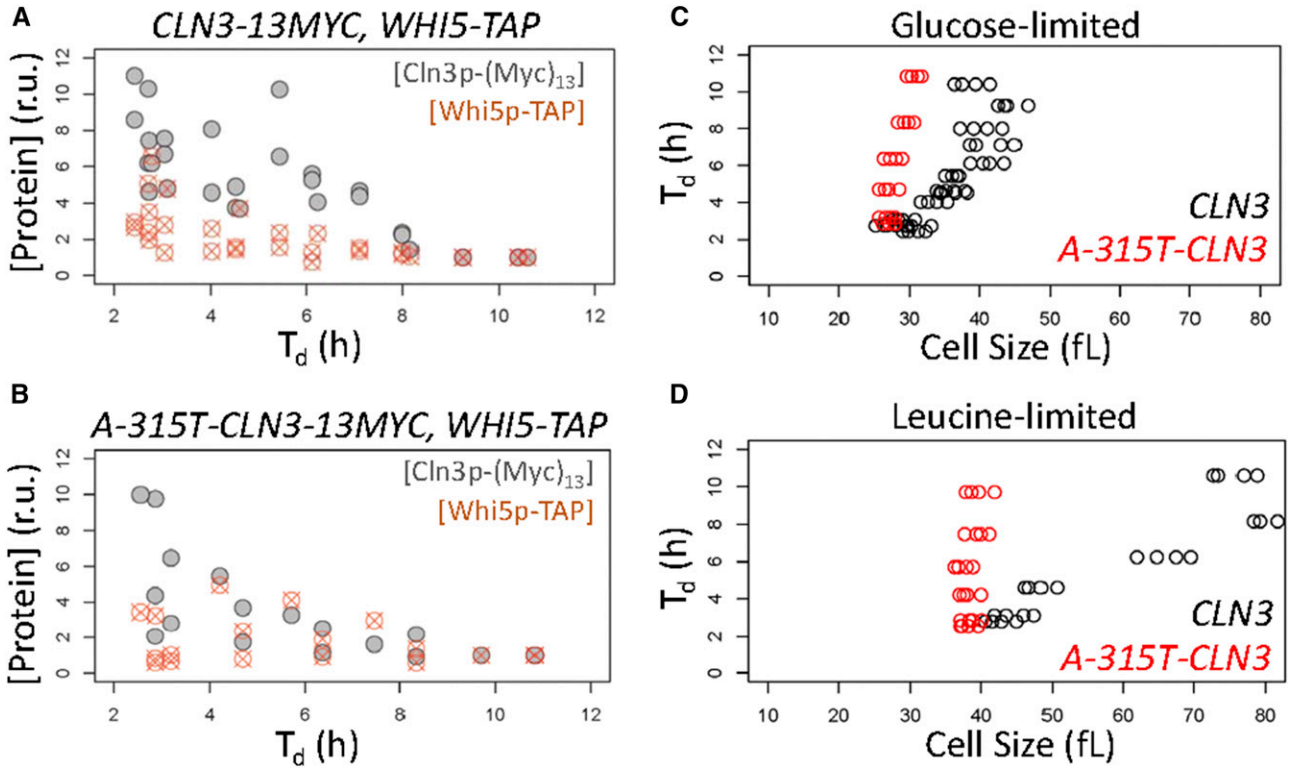

Figure 4 The levels of the G1 cyclin Cln3p vary over a broad range as a function of T_d, due to an upstream ORF (uORF) affecting translation of *CLN3*. Scatter plots of the relative abundance (*y*-axis) of Cln3p-$(Myc)_{13}$ and Whi5p-TAP in otherwise wild-type *CLN3-13MYC*, *WHI5-TAP* cells (A) or *CLN3* uORF (*A-315T-CLN3*) mutant cells (B), against T_d (*x*-axis). Each data point in the scatter plots is the average of immunoblot signal intensities run in duplicate, and detected with antibodies against the Myc or TAP epitopes (see *Materials and Methods*). All the raw immunoblots used to quantify protein levels are shown in the source data (File S1). Before averaging, each individual signal intensity value was normalized against loading in the corresponding immunoblot lane (visualized with Ponceau staining, see File S1 and *Materials and Methods*). For each Cln3p-$(Myc)_{13}$ or Whi5p-TAP relative unit (r.u.) shown in the scatterplots (A and B), the normalized, averaged intensities were scaled by the lowest value (set to 1) for each protein in the given chemostat experiment run at different dilution rates. Scatter plots of the relationship of cell size (*x*-axis) and T_d (*y*-axis) in the indicated strains, cultured under glucose (C) or leucine (D) limitation, from the same cultures described in (A) and (B).

breaks down in slower-proliferating *cln3*Δ cultures (Figure 3C and Figure S3, B and C). Even when combining all data points from the individual experiments for each strain, we found that at all doubling times tested the linear relationship between T_d, and that T_{G1} remains strong for *whi5*Δ cells ($\tau >$ 0.8, based on Kendall's nonparametric test). The same is true for *cln3*Δ cells at values of $LnT_d < 1.5$ (corresponding to T_d values <4.5 hr). In contrast, the linear relationship between T_d and T_{G1} is significantly weaker ($\tau < 0.5$) for slower-proliferating *cln3*Δ cells ($LnT_d > 1.5$). These data suggest that Cln3p is more important than Whi5p for imposing the proper scaling relationship of $T_d \propto T_{G1}$ in wild-type cells.

Cln3p levels are strongly and positively associated with cell proliferation rates

Given the important role of Cln3p in establishing the proper relationship between T_d and T_{G1} (Figure 3 and Figure S3), we sought to measure the levels of Cln3p and Whi5p as a function of T_d. There are no reports of the steady-state levels of Cln3p or Whi5p in cell populations proliferating at different rates in chemostats. To measure Whi5p and Cln3p levels from the same cells, we generated a strain that carries *WHI5-TAP* and *CLN3-13MYC* alleles, providing the only source of these gene products in the cells, expressed from their endogenous chromosomal locations (Figure 4A, see *Materials and Methods*). The expressed proteins were epitope-tagged, but otherwise unmutated, wild-type Whi5p-TAP and Cln3p-$(Myc)_{13}$. These cells were then cultured in continuous, steady-state chemostat cultures under glucose (0.08% $^{w}/_{v}$) or leucine (0.0015% $^{w}/_{v}$) limitation. Although the *CLN3-13MYC* allele provides the means for reliable detection of otherwise wild-type Cln3p, it is known to be slightly hypermorphic, stabilizing the Cln3p protein somewhat and shortening the G1 phase of the cell cycle (Thorburn *et al.* 2013). Indeed, the intercept of the linear fit between the log-transformed T_d and T_{G1} values of this strain (HB94; *WHI5-TAP* and *CLN3-13MYC*) was slightly higher than the intercept of the linear fit of these parameters in wild-type cells (0.97 *vs.* 0.92; see Table 1), consistent with a shortened G1 phase. The slope of the linear relationship between the log-transformed values of T_d and T_{G1} was increased somewhat for these cells compared to the aggregate analysis of wild-type cells (0.68 *vs.* 0.6; see Table 1). Importantly, these cells still displayed a strong, linear, positive

association between T_d and T_{G1} ($\tau = 0.77$; $r = 0.92$; see Table 1) at all dilution rates we tested. Hence, we concluded that the relationship between T_d and T_{G1} was only minimally affected in this strain, and we proceeded to quantify the levels of both Whi5p-TAP and Cln3p-$(Myc)_{13}$ from separate chemostat experiments under glucose or leucine limitation, each run at ≥ 5 dilution rates (Figure 4; see *Materials and Methods*).

The levels of Whi5p-TAP were not increased in slower-proliferating cells (Figure 4, A and B). Previously, (Liu *et al.* 2015) reported that Whi5p abundance increases around threefold in cells growing in poorer carbon sources, although this was not seen in a more recent study by Dorsey *et al.* (2018). In any case, several variables were different between the Liu *et al.* (2015) study and ours, which could account for the disagreement in the findings. First, different epitope-tagged alleles were used (*WHI5-tdTomato vs. WHI5-TAP*). Second, different detection methods were applied (fluorescence live cell imaging *vs.* immunoblots). Third, Liu *et al.* (2015) used cells in the W303 background, which are larger than cells of the BY background that we use here, possibly leading to differences in cell size regulation. Fourth, and most significantly, nutrient-specific effects could not be separated from growth rate-specific ones in Liu *et al.* (2015). As we discussed earlier (see Figure 2), chemostats provide the only experimental approach for properly studying how rates of cell proliferation may affect a given output, separately from any effects unique to particular nutrients.

We observed a significant and disproportionate reduction of Cln3p-$(Myc)_{13}$ levels in slower-proliferating cells (Figure 4, A and B). With Cln3p-$(Myc)_{13}$ levels normalized against the total cellular protein content, the fastest-proliferating populations had $>$ 10-fold higher levels of Cln3p-$(Myc)_{13}$ compared to the slowest-proliferating cells (Figure 4, A and B). Furthermore, because these estimates rely on the hypermorphic *CLN3-13MYC* allele, which produces a slightly stabilized Cln3p protein (Thorburn *et al.* 2013), the dynamic range of Cln3p levels as a function of doubling time is likely even broader.

A uORF in CLN3 adjusts the levels of Cln3p at different cell proliferation rates

What is the mechanism that underpins the growth-dependent control of Cln3p abundance? We had predicted that a uORF in *CLN3* could inhibit its translational efficiency in poor media disproportionately (Polymenis and Schmidt 1997). However, predictions of a growth-dependent role of the uORF had not been accompanied with measurements of Cln3p levels. A kinetic model of protein synthesis (Lodish 1974) forecasts that removing the uORF would derepress synthesis of Cln3p in slowly dividing cells when the ribosome content of the cell is low. In contrast, removing the *CLN3* uORF would have minimal effects in cells that proliferate quickly when the ribosome content is high. To test this model, we introduced an A-315T substitution that mutates the start codon of the uORF in *CLN3* without affecting *CLN3* mRNA levels (Polymenis and Schmidt 1997), in the strain that expresses otherwise wild-type Whi5p-TAP and Cln3p-$(Myc)_{13}$ (see *Materials and Methods*). Note also that in chemostat conditions very similar to the ones we used here, the levels of wild-type *CLN3* mRNA do not change significantly as a function of growth rate (Brauer *et al.* 2008).

The effects of the uORF were evident in slower-proliferating cultures ($T_d > 4$ hr), where the dynamic range of Cln3p levels was much narrower (three–fourfold) in A-315T cells, very different from the range of Cln3p levels (10-fold) in their wild-type counterparts at these longer doubling times ($P = 0.03648$, based on the nonparametric Kolmogorov–Smirnov test), and indistinguishable from the range of Whi5p levels (Figure 4, A and B and File S1). We note that although the range of Cln3p levels is narrower in slower-proliferating *CLN3* uORF mutant cells (Figure 4), it is not flattened, arguing for additional mechanisms that could adjust the levels of Cln3p at different growth rates. Nonetheless, an independent piece of functional evidence further strengthened a growth-dependent role of the *CLN3* uORF. A hallmark phenotypic readout of gain-of-function *CLN3* alleles is a reduction in cell size (Nash *et al.* 1988). Cells that lack the *CLN3* uORF were smaller than their wild-type counterparts were, and this effect was T_d-dependent (see Figure 4, C and D). Especially in leucine-limited cells, which displayed pronounced enlargement as they proliferated slower, removing the *CLN3* uORF reduced their size substantially (Figure 4D). These results are consistent with a derepression of Cln3p synthesis upon removal of the *CLN3* uORF.

These data argue that translational control contributes to the disproportionate reduction of Cln3p levels as a function of T_d. Note also that loss of Cln3p severely perturbs the linear relationship between T_d and T_{G1} (Figure 3 and Figure S3). In summary, our results underscore the critical role of the G1 cyclin Cln3p in the physiological coupling between growth and division.

Discussion

The scaling relationships between G1 length and population time in yeast and human cells that we report are significant for several reasons. First, if the duration of G1 is estimated, they allow predictions of proliferation rates, which could be useful in diverse settings, such as in tissues at an organismal level. Second, they serve as benchmarks against which the effects of genetic or other perturbations can be evaluated, as we demonstrated for Whi5p and Cln3p, two cell cycle regulators in yeast. Third, scaling relationships of cellular physiology may ultimately point to general, physical mechanisms that organize life at the cellular level. In the next paragraphs, we discuss our findings in relation to current models of how cell division is controlled by cellular biosynthetic capacity, with emphasis on the roles of Whi5p and Cln3p.

What is the context of this study in relation to others?

Our results pertain to cell cycle kinetics of steady-state cultures that proliferate at different rates, not to cell cycle

adjustments immediately after nutrient shifts (Tokiwa *et al.* 1994; Leitao and Kellogg 2017). We also did not examine G1 progression in a particular cell cycle, where small daughter cells will not initiate a new round of cell division until they reach a size characteristic of the culture medium (Hartwell and Unger 1977; Johnston *et al.* 1977). Hence, the scaling of G1 duration between populations with different doubling times may not necessarily be controlled by the same mechanism that controls how G1 duration is regulated to maintain size homeostasis within a population of cells that proliferates at a given rate. This interpretation is consistent with the findings that cell size is not associated with rates of cell proliferation (Figure 2), at least in experimental settings of steady-state chemostat cultures, which separate nutrient-specific effects from the impact of different rates of cell proliferation. For example, note the very different sizes of cells in glucose- *vs.* leucine-limited cultures at the same dilution rate (compare Figure 4, C and D), offering yet another demonstration of how particular nutrients may affect cell size independently of any changes in rates of cell proliferation. Furthermore, in leucine-limited cultures, the cells were not only bigger than cells in glucose-limited chemostats at all dilution rates tested, but they also got even bigger as they divided slower (Figure 4). These observations argue against the widely held assumptions that cells get smaller the slower they proliferate. Instead, they support the notion that nutrient effects on cell size may be particular to specific nutrients, and not associated with changes in rates of cell proliferation.

How do our results mesh with models of G1 control?

As we noted above, our data were from cells dividing at different rates, which was not addressed in the Whi5p dilution model of Schmoller *et al.* (2015). Hence, the two studies are not directly comparable. However, the Whi5p dilution model was constructed on the basis that while Whi5p levels were disproportionately lower than expected from cell growth, Cln3p levels were roughly constant and proportional to the increase in size from birth to START (Schmoller *et al.* 2015). Given the disproportionate dependency of Cln3p levels on cell proliferation rates that we reported here and had predicted earlier (Polymenis and Schmidt 1997), could the uORF-mediated translational control of *CLN3* affect Cln3p synthesis in the G1 phase from birth to START? We think this is unlikely because the uORF-mediated translational control we described operates when the concentration of active ribosomes in the cell changes (Lodish 1974), for example in poor *vs.* rich nutrients. Hence, while such translational control mechanisms provide excellent conduits to disproportionately alter gene expression and communicate growth-related inputs to downstream mRNA targets, to our knowledge, there is no report of cell cycle-dependent changes in ribosome content. Other mechanisms, not due to changes in the translational efficiency of *CLN3*, may contribute to significant, periodic changes in Cln3p abundance in G1, within a given cell cycle.

There are conflicting reports in the literature about whether Cln3p cycles in the cell cycle. Cln3p is of such low abundance that it could not be properly measured in the single-cell microscopy methods of Schmoller *et al.* (2015), because mutant *CLN3* alleles had to be used, producing extremely stabilized and dysfunctional Cln3p protein that accumulates at very high, but nonphysiological, levels so that it can be visible with microscopy. The initial report claiming that Cln3p-HA levels were constant in the cell cycle did not interrogate the early G1 phase (Tyers *et al.* 1993). In that report, although early G1, small (25 fl), elutriated daughter cells were collected, Cln3p levels were not measured until much later in G1 [at 35 fl, when by 40 fl, 25% of the cells were already budded in that experiment; see figure 4 in Tyers *et al.* (1993)]. Based on that result, it had been assumed for decades that Cln3p levels were constant in the cell cycle. However, two independent studies by the Amon (Thorburn *et al.* 2013) and Kellogg (Zapata *et al.* 2014) laboratories recently assayed elutriated synchronous cells carrying epitope-tagged, but otherwise wild-type, *CLN3* alleles. Both studies showed that Cln3p levels change $>$ 10-fold in G1. Cln3p is absent in early G1 cells, while it rises dramatically before START. We also used the same *CLN3-13MYC* allele to monitor Cln3p levels at different rates of cell proliferation (see Figure 4). The *CLN3-13MYC* allele is known to produce a slightly stabilized Cln3p protein (Thorburn *et al.* 2013). Note that, on the face of the slight stabilization of the Cln3p-$(Myc)_{13}$, the dynamic range of Cln3p levels as a function of growth rate that we report is likely even broader, not narrower. Hence, our conclusions are strengthened, not weakened, by the slight stabilization of the Cln3p-Myc we used. For the same reasons, the changes in Cln3p levels in G1 observed previously (Thorburn *et al.* 2013; Zapata *et al.* 2014) are likely even greater than indicated in these reports.

Overall, although a twofold dilution of Whi5p is observed in G1 (Schmoller *et al.* 2015), the changes in Cln3p levels are likely more pronounced (Thorburn *et al.* 2013; Zapata *et al.* 2014), through transcriptional (Zapata *et al.* 2014) or other mechanisms. In this context, it is perhaps unsurprising that we found Cln3p to be more important than Whi5p in the relationship between T_d and T_{G1}. However, it is important to stress that any changes of Cln3p levels in G1 do not affect the key aspect of the inhibitor dilution model, namely that Whi5p levels are reduced by cell growth. Hence, we may be dealing with a more complex, "mixed" model of inhibitor dilution *and* activator accumulation. It is possible that the levels of additional proteins may behave analogously to Cln3p and Whi5p, contributing to a broader network of factors whose antagonistic relationships control the timing of initiation of cell division. Regardless of the identity of those proteins, in yeast and other models, the fundamental relationship between T_{G1} and T_d we describe in this report will serve as a useful metric to evaluate the role of these protein(s) in the control of cell division by growth inputs.

Acknowledgments

This work was supported by the National Institutes of Health (grant GM-123139 to M.P.). M.C. was supported

by a National Science Foundation Research Experience for Undergraduates (REU) award (DBI-1358941). The authors declare no conflicts of interest.

Author contributions: H.M.B. and M.P. devised the methodology. H.M.B. and M.P. performed formal analysis. H.M.B., M.C., I.P.E.P., A.O.P., and M.P. conducted the investigation. M.P. secured resources. H.M.B. and M.P. provided data curation. M.P. wrote the original draft of the manuscript. H.M.B. and M.P. reviewed and edited the manuscript. H.M.B. and M.P. conducted visualization. H.M.B. and M.P. supervised the project. M.P. was responsible for funding acquisition.

Literature Cited

Anastasia, S. D., D. L. Nguyen, V. Thai, M. Meloy, T. MacDonough *et al.*, 2012 A link between mitotic entry and membrane growth suggests a novel model for cell size control. J. Cell Biol. 197: 89–104. https://doi.org/10.1083/jcb.201108108

Aoki, Y., and G. E. Moore, 1970 Comparative study of mitotic stages of cells derived from human peripheral blood. Exp. Cell Res. 59: 259–266. https://doi.org/10.1016/0014-4827(70)90599-9

Baserga, R., 1985 The Biology of Cell Reproduction. Harvard University Press, Cambridge, MA.

Blank, H. M., R. Perez, C. He, N. Maitra, R. Metz *et al.*, 2017 Translational control of lipogenic enzymes in the cell cycle of synchronous, growing yeast cells. EMBO J. 36: 487–502. https://doi.org/10.15252/embj.201695050

Borenstein, M., 2009 *Introduction to Meta-Analysis*. John Wiley & Sons, Chichester, U.K. https://doi.org/10.1002/9780470743386

Brauer, M. J., C. Huttenhower, E. M. Airoldi, R. Rosenstein, J. C. Matese *et al.*, 2008 Coordination of growth rate, cell cycle, stress response, and metabolic activity in yeast. Mol. Biol. Cell 19: 352–367. https://doi.org/10.1091/mbc.e07-08-0779

Brons, P. P., J. M. Raemaekers, M. J. Bogman, P. E. van Erp, J. B. Boezeman *et al.*, 1992 Cell cycle kinetics in malignant lymphoma studied with in vivo iododeoxyuridine administration, nuclear Ki-67 staining, and flow cytometry. Blood 80: 2336–2343.

Bryan, A. K., A. Engler, A. Gulati, and S. R. Manalis, 2012 Continuous and long-term volume measurements with a commercial Coulter counter. PLoS One 7: e29866. https://doi.org/10.1371/journal.pone.0029866

Cerulus, B., A. M. New, K. Pougach, and K. J. Verstrepen, 2016 Noise and epigenetic inheritance of single-cell division times influence population fitness. Curr. Biol. 26: 1138–1147. https://doi.org/10.1016/j.cub.2016.03.010

Chan, Y. H., and W. F. Marshall, 2010 Scaling properties of cell and organelle size. Organogenesis 6: 88–96. https://doi.org/10.4161/org.6.2.11464

Costanzo, M., J. L. Nishikawa, X. Tang, J. S. Millman, O. Schub *et al.*, 2004 CDK activity antagonizes Whi5, an inhibitor of G1/S transcription in yeast. Cell 117: 899–913. https://doi.org/10.1016/j.cell.2004.05.024

Cross, F. R., 1988 DAF1, a mutant gene affecting size control, pheromone arrest, and cell cycle kinetics of Saccharomyces cerevisiae. Mol. Cell. Biol. 8: 4675–4684. https://doi.org/10.1128/MCB.8.11.4675

de Bruin, R. A., W. H. McDonald, T. I. Kalashnikova, J. Yates, III, and C. Wittenberg, 2004 Cln3 activates G1-specific transcription via phosphorylation of the SBF bound repressor Whi5. Cell 117: 887–898. https://doi.org/10.1016/j.cell.2004.05.025

Defendi, V., and L. A. Manson, 1963 Analysis of the life-cycle in mammalian cells. Nature 198: 359–361. https://doi.org/10.1038/198359a0

Di Talia, S., J. M. Skotheim, J. M. Bean, E. D. Siggia, and F. R. Cross, 2007 The effects of molecular noise and size control on variability in the budding yeast cell cycle. Nature 448: 947–951 (erratum: Nature 450: 1272). https://doi.org/10.1038/nature06072

Dorsey, S., S. Tollis, J. Cheng, L. Black, S. Notley *et al.*, 2018 G1/S transcription factor copy number is a growth-dependent determinant of cell cycle commitment in yeast. Cell Syst. 6: 539–554. e11. https://doi.org/10.1016/j.cels.2018.04.012

Dowling, M. R., A. Kan, S. Heinzel, J. H. Zhou, J. M. Marchingo *et al.*, 2014 Stretched cell cycle model for proliferating lymphocytes. Proc. Natl. Acad. Sci. USA 111: 6377–6382. https://doi.org/10.1073/pnas.1322420111

Elliott, S. G., and C. S. McLaughlin, 1978 Rate of macromolecular synthesis through the cell cycle of the yeast Saccharomyces cerevisiae. Proc. Natl. Acad. Sci. USA 75: 4384–4388. https://doi.org/10.1073/pnas.75.9.4384

Ferrezuelo, F., N. Colomina, A. Palmisano, E. Gari, C. Gallego *et al.*, 2012 The critical size is set at a single-cell level by growth rate to attain homeostasis and adaptation. Nat. Commun. 3: 1012. https://doi.org/10.1038/ncomms2015

Fisher, R. P., 2016 Getting to S: CDK functions and targets on the path to cell-cycle commitment. F1000 Res. 5: 2374. https://doi.org/10.12688/f1000research.9463.1

Garmendia-Torres, C., O. Tassy, A. Matifas, N. Molina, and G. Charvin, 2018 Multiple inputs ensure yeast cell size homeostasis during cell cycle progression. Elife 7: e34025. https://doi.org/10.7554/eLife.34025

Garner, K. M., and A. Eastman, 2011 Variations in Mre11/Rad50/Nbs1 status and DNA damage-induced S-phase arrest in the cell lines of the NCI60 panel. BMC Cancer 11: 206. https://doi.org/10.1186/1471-2407-11-206

Guo, J., B. A. Bryan, and M. Polymenis, 2004 Nutrient-specific effects in the coordination of cell growth with cell division in continuous cultures of Saccharomyces cerevisiae. Arch. Microbiol. 182: 326–330. https://doi.org/10.1007/s00203-004-0704-2

Hahn, A. T., J. T. Jones, and T. Meyer, 2009 Quantitative analysis of cell cycle phase durations and PC12 differentiation using fluorescent biosensors. Cell Cycle 8: 1044–1052. https://doi.org/10.4161/cc.8.7.8042

Hartwell, L. H., and M. W. Unger, 1977 Unequal division in Saccharomyces cerevisiae and its implications for the control of cell division. J. Cell Biol. 75: 422–435. https://doi.org/10.1083/jcb.75.2.422

Henry, K. A., H. M. Blank, S. A. Hoose, and M. Polymenis, 2010 The unfolded protein response is not necessary for the G1/S transition, but it is required for chromosome maintenance in Saccharomyces cerevisiae. PLoS One 5: e12732. https://doi.org/10.1371/journal.pone.0012732

Hoffman, J. G., 1949 Theory of the mitotic index and its application to tissue growth measurement. Bull. Math. Biophys. 11: 139–144. https://doi.org/10.1007/BF02477499

Hoose, S. A., J. A. Rawlings, M. M. Kelly, M. C. Leitch, Q. O. Ababneh *et al.*, 2012 A systematic analysis of cell cycle regulators in yeast reveals that most factors act independently of cell size to control initiation of division. PLoS Genet. 8: e1002590. https://doi.org/10.1371/journal.pgen.1002590

Hoose, S. A., J. T. Trinh, M. C. Leitch, M. M. Kelly, R. F. McCormick *et al.*, 2013 Saccharomyces cerevisiae deletion strains with complex DNA content profiles. FEMS Microbiol. Lett. 345: 72–76. https://doi.org/10.1111/1574-6968.12186

Jagadish, M. N., and B. L. Carter, 1977 Genetic control of cell division in yeast cultured at different growth rates. Nature 269: 145–147. https://doi.org/10.1038/269145a0

Johnston, G., R. Singer, S. Sharrow, and M. Slater, 1980 Cell division in the yeast Saccharomyces cerevisiae growing at different rates. Microbiology 118: 479–484. https://doi.org/10.1099/00221287-118-2-479

Johnston, G. C., J. R. Pringle, and L. H. Hartwell, 1977 Coordination of growth with cell division in the yeast Saccharomyces cerevisiae. Exp. Cell Res. 105: 79–98. https://doi.org/10.1016/0014-4827(77)90154-9

Koch, A. L., 1966 The logarithm in biology. 1. Mechanisms generating the log-normal distribution exactly. J. Theor. Biol. 12: 276–290. https://doi.org/10.1016/0022-5193(66)90119-6

Koch, A. L., and M. Schaechter, 1962 A model for statistics of the cell division process. J. Gen. Microbiol. 29: 435–454. https://doi.org/10.1099/00221287-29-3-435

Kumei, Y., T. Nakajima, A. Sato, N. Kamata, and S. Enomoto, 1989 Reduction of G1 phase duration and enhancement of c-myc gene expression in HeLa cells at hypergravity. J. Cell Sci. 93: 221–226.

Leitao, R. M., and D. R. Kellogg, 2017 The duration of mitosis and daughter cell size are modulated by nutrients in budding yeast. J. Cell Biol. 216: 3463–3470. https://doi.org/10.1083/jcb.201609114

Lennartz, K. J., and W. Maurer, 1964 Autoradiographische Bestimmung der Dauer der DNS-Verdopplung und der Generationszeit beim Ehrlich-Ascitestumor der Maus durch Doppelmarkierung mit 14C- und ^{3}H-Thymidin. Z. Zellforsch. Mikrosk. Anat. 63: 478–495. https://doi.org/10.1007/BF00339486

Liu, X., X. Wang, X. Yang, S. Liu, L. Jiang *et al.*, 2015 Reliable cell cycle commitment in budding yeast is ensured by signal integration. Elife 4: e03977. https://doi.org/10.7554/eLife.03977

Lodish, H. F., 1974 Model for the regulation of mRNA translation applied to haemoglobin synthesis. Nature 251: 385–388. https://doi.org/10.1038/251385a0

Luciani, A. M., A. Rosi, P. Matarrese, G. Arancia, L. Guidoni *et al.*, 2001 Changes in cell volume and internal sodium concentration in HeLa cells during exponential growth and following lonidamine treatment. Eur. J. Cell Biol. 80: 187–195. https://doi.org/10.1078/0171-9335-00102

Mayhew, M. B., E. S. Iversen, and A. J. Hartemink, 2017 Characterization of dependencies between growth and division in budding yeast. J. R. Soc. Interface 14: 20160993. https://doi.org/10.1098/rsif.2016.0993

Morgan, D. O., 2007 Control of cell proliferation and growth, pp. 221 in *The Cell Cycle*. New Science Press Ltd, London.

Mosimann, J. E., and G. Campbell, 1988 Applications in biology: simple growth models, pp. 287–302 in *Lognormal Distributions: Theory and Applications*, edited by E. Crow, L. Shimizu, and K. Marcel. Dekker, Inc., New York.

Nash, R., G. Tokiwa, S. Anand, K. Erickson, and A. B. Futcher, 1988 The WHI1+ gene of Saccharomyces cerevisiae tethers cell division to cell size and is a cyclin homolog. EMBO J. 7: 4335–4346.

Palumbo, P., M. Vanoni, V. Cusimano, S. Busti, F. Marano *et al.*, 2016 Whi5 phosphorylation embedded in the G1/S network dynamically controls critical cell size and cell fate. Nat. Commun. 7: 11372. https://doi.org/10.1038/ncomms11372

Peña, E. A., and E. H. Slate, 2006 Global validation of linear model assumptions. J. Am. Stat. Assoc. 101: 341–354. https://doi.org/10.1198/016214505000000637

Polymenis, M., 2017 Proteins associated with the doubling time of the NCI-60 cancer cell lines. Cell Div. 12: 6. https://doi.org/10.1186/s13008-017-0032-y

Polymenis, M., and E. V. Schmidt, 1997 Coupling of cell division to cell growth by translational control of the G1 cyclin CLN3 in yeast. Genes Dev. 11: 2522–2531. https://doi.org/10.1101/gad.11.19.2522

Rivin, C. J., and W. L. Fangman, 1980 Cell cycle phase expansion in nitrogen-limited cultures of Saccharomyces cerevisiae. J. Cell Biol. 85: 96–107. https://doi.org/10.1083/jcb.85.1.96

Ross, D. T., U. Scherf, M. B. Eisen, C. M. Perou, C. Rees *et al.*, 2000 Systematic variation in gene expression patterns in human cancer cell lines. Nat. Genet. 24: 227–235. https://doi.org/10.1038/73432

Scherf, U., D. T. Ross, M. Waltham, L. H. Smith, J. K. Lee *et al.*, 2000 A gene expression database for the molecular pharmacology of cancer. Nat. Genet. 24: 236–244. https://doi.org/10.1038/73439

Schmoller, K. M., and J. M. Skotheim, 2015 The biosynthetic basis of cell size control. Trends Cell Biol. 25: 793–802. https://doi.org/10.1016/j.tcb.2015.10.006

Schmoller, K. M., J. J. Turner, M. Koivomagi, and J. M. Skotheim, 2015 Dilution of the cell cycle inhibitor Whi5 controls budding-yeast cell size. Nature 526: 268–272. https://doi.org/10.1038/nature14908

Siegel, A. F., 1982 Robust regression using repeated medians. Biometrika 69: 242–244. https://doi.org/10.1093/biomet/69.1.242

Sisken, J. E., and R. Kinosita, 1961 Timing of DNA synthesis in the mitotic cycle in vitro. J. Biophys. Biochem. Cytol. 9: 509–518. https://doi.org/10.1083/jcb.9.3.509

Slater, M. L., S. O. Sharrow, and J. J. Gart, 1977 Cell cycle of Saccharomycescerevisiae in populations growing at different rates. Proc. Natl. Acad. Sci. USA 74: 3850–3854. https://doi.org/10.1073/pnas.74.9.3850

Soifer, I., and N. Barkai, 2014 Systematic identification of cell size regulators in budding yeast. Mol. Syst. Biol. 10: 761. https://doi.org/10.15252/msb.20145345

Soma, S., K. Yang, M. I. Morales, and M. Polymenis, 2014 Multiple metabolic requirements for size homeostasis and initiation of division in Saccharomyces cerevisiae. Microb. Cell 1: 256–266. https://doi.org/10.15698/mic2014.08.160

Son, S., A. Tzur, Y. Weng, P. Jorgensen, J. Kim *et al.*, 2012 Direct observation of mammalian cell growth and size regulation. Nat. Methods 9: 910–912. https://doi.org/10.1038/nmeth.2133

Thorburn, R. R., C. Gonzalez, G. A. Brar, S. Christen, T. M. Carlile *et al.*, 2013 Aneuploid yeast strains exhibit defects in cell growth and passage through START. Mol. Biol. Cell 24: 1274–1289. https://doi.org/10.1091/mbc.e12-07-0520

Tokiwa, G., M. Tyers, T. Volpe, and B. Futcher, 1994 Inhibition of G1 cyclin activity by the Ras/cAMP pathway in yeast. Nature 371: 342–345. https://doi.org/10.1038/371342a0

Tyers, M., G. Tokiwa, and B. Futcher, 1993 Comparison of the Saccharomyces cerevisiae G1 cyclins: Cln3 may be an upstream activator of Cln1, Cln2 and other cyclins. EMBO J. 12: 1955–1968.

Tyson, C. B., P. G. Lord, and A. E. Wheals, 1979 Dependency of size of Saccharomyces cerevisiae cells on growth rate. J. Bacteriol. 138: 92–98.

Tzur, A., R. Kafri, V. S. LeBleu, G. Lahav, and M. W. Kirschner, 2009 Cell growth and size homeostasis in proliferating animal cells. Science 325: 167–171. https://doi.org/10.1126/science.1174294

Viechtbauer, W., 2010 Conducting meta-analyses in R with the metafor package. J. Stat. Softw. 36: 1–48. https://doi.org/10.18637/jss.v036.i03

Zapata, J., N. Dephoure, T. Macdonough, Y. Yu, E. J. Parnell *et al.*, 2014 PP2ARts1 is a master regulator of pathways that control cell size. J. Cell Biol. 204: 359–376. https://doi.org/10.1083/jcb.201309119

Communicating editor: A. Gladfelter